

# Two-dimensional plumes in stratified environments

By PETER G. BAINES

CSIRO Division of Atmospheric Research, Aspendale 3195, Australia

(Received 27 July 2001 and in revised form 10 May 2002)

Laboratory experiments on the flow of negatively buoyant two-dimensional plumes adjacent to a wall in a density-stratified environment are described. The flow passes through several stages, from an inertial jet to a buoyant plume, to a neutrally buoyant jet, and then a negatively buoyant plume when it overshoots its equilibrium density. This fluid then ‘springs back’ and eventually occupies an intermediate range of heights. The flow is primarily characterized by the initial value of the buoyancy number,  $B_0 = Q_0 N^3 / g_0'^2$ , where  $Q_0$  is the initial volume flux per unit width,  $g_0'$  is the initial buoyancy and  $N$  is the buoyancy frequency of the environment. Scaled with the initial equilibrium depth  $D$  of the inflowing fluid, the maximum depth of penetration increases with  $B_0$ , as does the width of the initial downflow, which is observed to increase very slowly with distance downward. Observations are made of the profiles of flow into and away from the plume as a function of height. Various properties of the flow are compared with predictions from the ‘standard’ two-dimensional entraining plume model, and this shows generally consistent agreement, although there are differences in magnitudes and in details. This flow contrasts with flows down gentle slopes into stratified environments, where two-way exchange of fluid occurs.

---

## 1. Introduction

Plumes are defined as buoyant jets where the initial jet momentum is not significant, or has become completely dominated by the buoyancy force. Man-made examples are the plumes from chimneys in the atmosphere, and buoyant sewage outfalls in the ocean. Several naturally occurring phenomena can be modelled as buoyant jets and plumes. In the atmosphere, these include flow above isolated radiatively heated regions of the earth’s surface, above fires and volcanoes, and in the ocean, flow below isolated regions of surface cooling (Killworth 1979), and above fissures in mid-ocean ridges (Palmer & Ernst 1998). In many of these naturally occurring examples, the variation of the background potential density with height (the density stratification) is important in the overall dynamics, and the flow tends to have a two-dimensional character rather than an axisymmetric one. Examples are flow above advancing fires, above hot fissures in mid-ocean ridges, and below leads in ice sheets on the ocean surface. There have been several reviews of the dynamics of jets and plumes (Chen & Rodi 1980; List 1982*a, b*). In particular, List (1982*a*) has pointed out that the properties of non-buoyant jets are much better understood than those of buoyant jets and plumes. Most studies of buoyant jets have been with homogeneous environments, and this applies to the experiments on two-dimensional buoyant jets (Rouse, Yih & Humphreys 1952; Kotsovinos & List 1977).

The present study is based on experiments on two-dimensional buoyant jets into

strongly stratified environments, and is focused on the effects of stratification. It is part of a more extensive study of downslope flows into stratified environments, of which a preliminary report is given in Baines (1999), and results for gentle slopes are described in Baines (2001). The buoyant jets described here are the limiting case of flow down a 'slope' that is vertical, and are reported separately because of their significance in other contexts. These experiments are therefore for one-sided two-dimensional buoyant jets, where large-scale meandering (Kotsovinos 1977) is suppressed, and this should be borne in mind when comparisons are made. The only significant experiments to date on plumes into open stratified environments are those of Morton, Taylor & Turner (1956) who used axisymmetric sources, and Bloomfield & Kerr (1998), who used axisymmetric and line sources. Morton *et al.* introduced the concept of *turbulent entrainment* of environmental fluid into the plume, where the inflow  $V_E$  is proportional to the mean axial velocity in the plume,  $U$ . The ratio of these two quantities is the entrainment constant,  $E$ , so that  $V_E = EU$ . This concept and assumption has now become widely accepted and used, with the modification that the entrainment 'constant' is seen to be a function of the relevant dimensionless variables (List & Imberger 1973), most notably the bulk pseudo-Richardson number  $R_p$  of the jet or plume, where  $R_p = g'b/U^2$ . This quantity has sometimes been termed the 'Richardson number', though given the orientation of the flow, it is not a Richardson number in the usual sense because here buoyancy is driving the flow rather than acting to stabilize it. For this reason the term 'pseudo-Richardson number' has been used. Here,  $b$  is the local radius of the plume and  $G \equiv g' \equiv g\Delta\rho/\bar{\rho}_e$  is its local buoyancy,  $g$  is the acceleration due to gravity,  $\bar{\rho}_e$  is the mean environmental density and  $\Delta\rho$  is the local difference between the density of fluid in the plume and in the environment. The entrainment is therefore dependent on local conditions, varies with height in the plume, and stems from the similarity properties of the turbulence associated with the large-scale properties of the plume. For two-dimensional buoyant jets, the entrainment constant varies by a factor of two from jets to plumes (Kotsovinos & List 1977), but may be regarded as a constant for pure jets or pure plumes. This applies to both axisymmetric and two-dimensional jets or plumes, but the values of the entrainment constant are different for all four cases.

Morton *et al.* (1956) also introduced a theoretical model for axisymmetric plumes that incorporates this entrainment assumption, and consists of equations for conservation of the fluxes of mass, momentum and buoyancy, integrated horizontally across the plume. If we allow for the dependence of entrainment on  $R_p$ , this model is essentially equivalent to a model of Priestley & Ball (1955) that uses slightly different assumptions and equations (List & Imberger 1973). However, the model of Morton *et al.* (1956) invoking the assumption of turbulent entrainment has been preferred for subsequent work and application because of its conceptual simplicity (Turner 1986). For stratified environments, Morton *et al.* (1956) reported that, after rising in the plume, the inflowing fluid was deposited over a range of heights that lay below the maximum plume height. They identified the upper boundary of this range with the height in the model where the velocity  $U$  had been reduced to zero by the reversal of buoyancy, and they inferred the value of the entrainment constant for axisymmetric plumes from these measured heights of rise.

Bloomfield & Kerr (1998) observed the properties of 'fountains', in which negatively buoyant fluid is injected upward, in a stratified environment, and compared their results with the same bulk model described by Morton *et al.* (1956). For both the axisymmetric and two-dimensional versions, reasonable consistency between the model and the observations was obtained, provided the value of the entrainment

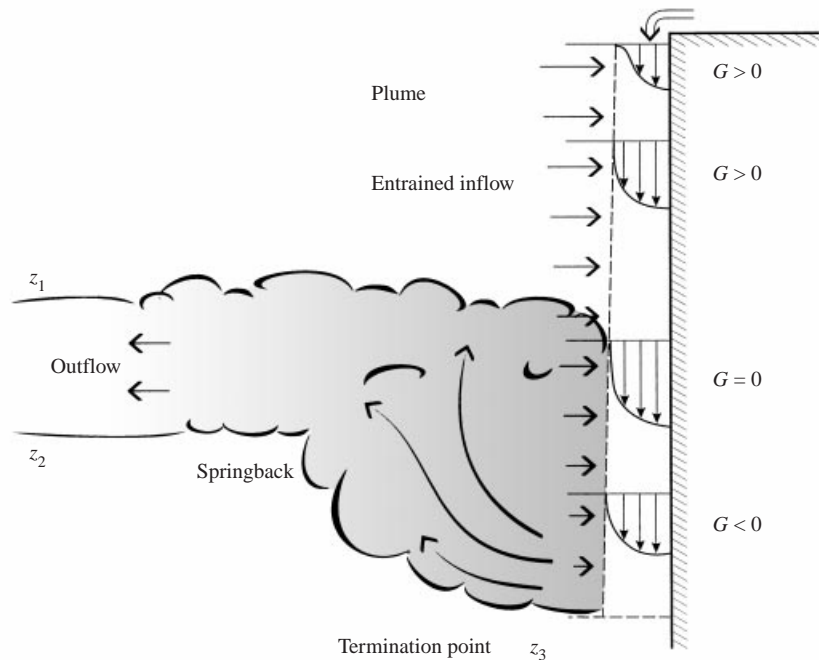


FIGURE 1. Schematic diagram showing the nature of the flow in a typical experiment.  $G$  denotes the buoyancy (positive downwards) of the fluid in the downflowing plume relative to the local stratified environment, and the horizontal arrows denote the entrained inflow.  $z_1$  and  $z_2$  denote the upper and lower levels of the net outflow, and  $z_3$  denotes the level of maximum downward extent of the plume.

constant ( $E = 0.08$ ) was chosen to give agreement between the theoretical predictions and observed values of the maximum height of the fountain.

Similar properties to those described by Morton *et al.* (1956) and Bloomfield & Kerr (1998) are seen in the present experiments. A representative schematic diagram of a typical experiment is shown in figure 1. The fluid in the plume is ultimately deposited within a distinct range of depths, and the maximum depth of penetration is again larger than this range because of the 'overshoot and springback' phenomenon. The plume penetrates well below its level of neutral buoyancy (beyond which it may be regarded as a 'fountain') to a level  $z_3$ , where  $z$  is the vertical coordinate with positive direction upwards. The fluid in the plume then springs back to be deposited within the range between heights  $z_1$  and  $z_2$ , where  $|z_1| < |z_2| < |z_3|$  (here the origin of  $z$  is taken near the source, and since the plume is negatively buoyant,  $z$  is negative). No inflowing or entrained fluid is deposited beyond height  $z_2$ , but some environmental fluid from this range is entrained and mixed into the plume, and is then carried into the range between  $z_1$  and  $z_2$  with the springback process. These observations are described in detail in §3. The two-dimensional version of the 'standard' plume model is outlined and compared with observations in §4, and the conclusions are summarized in §5. As in Baines (2001), the principal parameter governing the flow is seen to be the dimensionless number  $B_0$ , the initial value of the parameter  $B$ , which may be termed the 'Buoyancy number' of the current, or plume. In previous publications this parameter was termed  $M$ , but has been altered here on the recommendation of the editor and referees, in the interests of optimizing

terminology in the subject.  $B_0$  is defined as

$$B_0 = \frac{Q_0}{(g'_0 D^3)^{1/2}} = \frac{Q_0 N_0^3}{g_0'^2}, \quad (1.1)$$

where  $Q_0$  and  $g'_0$  denote the initial volume flux (per unit length) and buoyancy of the plume, respectively.  $N$  denotes the buoyancy frequency of the environmental fluid, defined by  $N^2 = -(g/\bar{\rho}_e) d\rho_e/dz$ , where  $\rho_e(z)$  is the environmental density profile.  $N_0$  denotes the mean value of  $N$  over the range of depths of interest, defined by

$$N_0^2 = \frac{g\Delta\rho}{\bar{\rho}_e D} = \frac{g'_0}{D}, \quad (1.2)$$

where  $D$  denotes the distance below the source at which the density of the environmental fluid is equal to that of the initial fluid released in the plume. If  $N$  is uniform with height, we have  $N = N_0$ . A second parameter that is required to characterize the overall flow is the initial pseudo-Richardson number

$$R_{p0} = g'_0 \bar{d}(0)^3 / Q_0^2, \quad (1.3)$$

where  $\bar{d}$  denotes the mean thickness of the plume (averaging over eddies) and  $\bar{d}(0)$  is its initial value. If viscosity is important, the Reynolds number

$$Re = \frac{Q_0}{\nu}, \quad (1.4)$$

is also significant, but this is not the case for most flows described here, where  $Re$  exceeds values of several hundred. Local values of  $B$ ,  $R_p$  and  $Re$  may also be defined in terms of local values of  $Q$ ,  $G$  and  $\bar{d}$ , as given in §3. Of these parameters,  $R_{p0}$  and  $Re$  are well known and their significance requires no discussion here (see e.g. List & Imberger 1973; List 1982*a, b*).  $B_0$  has values that typically range from 0.001 to 0.1, in both laboratory and environmental situations.  $B$  may be regarded as a measure of the relative importance of stratification to the dynamics of the plume, and is the cube of the ratio of two time scales: the time scale of the gravity current  $(Q/G^2)^{1/3}$ , and that of the ambient stratification,  $1/N$ . Alternatively,  $B$  may be interpreted as (the cube of) the ratio of two length scales:  $(Q^2/G)^{1/3}$ , the intrinsic scale of the plume, to  $L_n = (QG)^{1/3}/N$ , the characteristic scale of height of rise from a source of buoyancy in a stratified environment.

## 2. Experiments

The experiments were carried out in the tank and configuration illustrated in figure 2. The glass-sided tank was approximately 80 cm high and rectangular in cross-section, with internal dimensions of 299 cm in length and 38 cm in width, open at the top and with a solid horizontal bottom. In order to increase the effective working length of the tank (as explained below), a thin vertical Perspex partition was placed in the tank extending from one end along approximately 80% of its length, with a uniform gap width of 23 cm on one side and 15 cm on the other. The main working region of the tank was in the wider region of width 23 cm, and the experiment was made two-dimensional in this portion as much as possible. A horizontal platform 45 cm above the floor of the tank and extending 40 cm from one end (on the right-hand side in figure 2) was inserted in the working region. This was terminated by a vertical wall extending downward from the platform to the floor of the tank, and after the tank was filled, the region beneath the platform was sealed off from the remainder

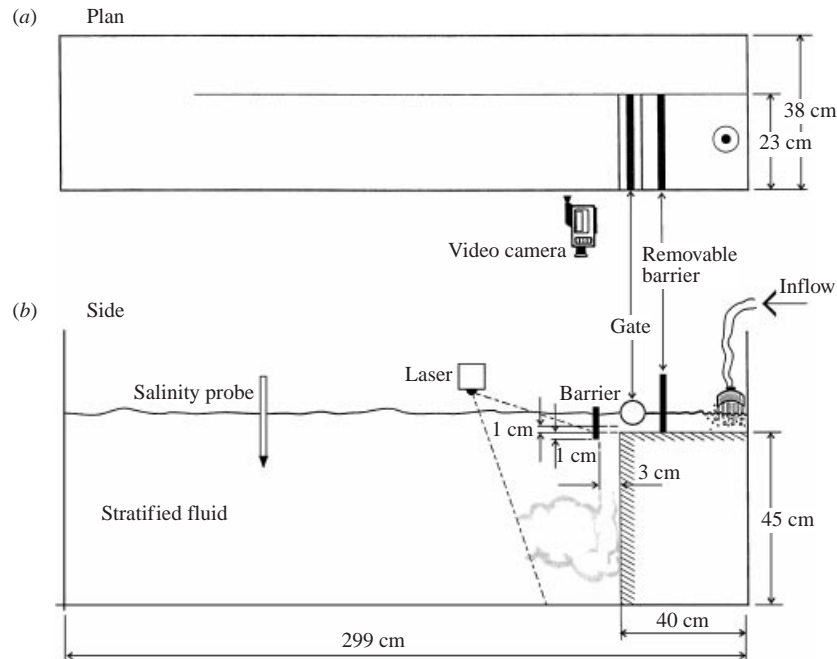


FIGURE 2. Schematic diagram of the experimental apparatus. (a) Plan view, (b) side view.

of the tank. A fixed gate (or contraction) consisting of a horizontal cylinder (radius 2 cm) spanning the working region perpendicular to the sidewalls, and leaving a gap of 1 cm between it and the platform below, was placed with its centre at a distance of 39 cm from the end of the tank, 1 cm from the vertical wall. Before the experiments, the tank was filled to a level above this gap, with uniformly salt-stratified fluid, using the customary two-tank mixing procedure. During filling, the region beneath the platform (behind the vertical wall) was connected with the main volume of the tank by openings in the central vertical barrier and in the platform, in order to give a uniform density stratification (particularly at the platform level) from the filling process; these openings were then sealed after filling and before experimental runs. A removable sealed vertical barrier was placed at approximately 1 cm away from the gate, on the shallow side, isolating the fluid above the platform from the remainder of the tank.

When an experiment was begun, the vertical barrier was removed and a continuous supply of dense fluid was provided at a constant flow rate to the region above the platform behind the gate. This geometry therefore had the effect of providing a two-dimensional source, uniform across the working region and flowing into the deeper region from under the gate, with an abrupt, sudden commencement. The presence of the gate prevented the lighter fluid in the deeper part of the tank from entering the shallow region above the platform, and helped to ensure that the source flow was uniform across the working region.

The stationary fluid in the tank was stratified with a vertical density profile  $\rho_0(z)$ , where  $z$  is the vertical coordinate, positive upwards with the origin taken at the level of the platform of the source fluid. In all runs, the density gradient was uniform with depth, so that the buoyancy frequency  $N$ , given by (1.2), was effectively constant. The density  $\rho_i$  of the inflowing fluid was equal to the initial ambient density at a

$B_0$	$Q_0$ ( $\text{cm}^2 \text{s}^{-1}$ )	$g'_0$ ( $\text{cm s}^{-2}$ )	$N$ ( $\text{s}^{-1}$ )	$D$ (cm)	$Re$	$\bar{d}$ (cm)	$R_{p0}$	$T$ (s)
0.00175	2.697	40.87	1.03	38.7	269.7	0.9	4.1	240
0.00216	2.697	34.40	0.982	35.68	269.7	1.2	8.2	240
0.00302	2.697	18.91	0.737	34.82	269.7	1.5	8.8	240
0.00446	4.091	17.47	0.693	36.38	409.1	1.5	3.5	165
0.00458	10.368	30.84	0.749	55	1036.8	2.9	7.0	90
0.00636	4.091	7.91	0.460	37.39	409.1	2.3	5.75	165
0.00687	5.486	19.56	0.783	31.94	548.6	1.7	3.2	120
0.00925	10.368	28.41	0.896	35.36	1036.8	2	2.1	90
0.0218	6.88	12.59	0.793	19.93	688	2	2.1	90
0.0258	8.275	10.02	0.679	21.75	827.5			90
0.0633	13.854	11.66	0.853	16.02	1385.4	3	1.6	45
0.0852	13.854	6.62	0.646	15.86	1385.4	3	0.93	45
0.0877	13.854	5.36	0.566	16.7	1385.4	3	0.75	45
0.0986	13.854	4.59	0.531	16.27	1385.4	3	0.65	45

TABLE 1. Parameter values for the 14 runs analysed in this paper.  $T$  denotes the length of time of inflow, and  $R_{p0}$  is here given by equation (1.3), using the observed values of  $\bar{d}$  for  $\bar{d}(0)$ .

level  $D$  below the level of the source, so that  $\rho_i = \rho_0(-D)$ . For most runs, the dense inflow descended directly adjacent to the vertical wall under the influence of gravity, as a turbulent negatively buoyant jet. This behaviour was assisted by inserting a short vertical barrier (see figure 2) at a distance of 3 cm from the wall, that extended 1 cm below the level of the platform. For low flow rates, this barrier had no effect and was not required. In runs with large flow rates without the barrier, the dense inflow entered the tank more horizontally and remained separated from the wall for a substantial time; runs with this behaviour had different character and were excluded from analysis. Adding the short barrier effectively prevented this initial separation, and gave an attached buoyant jet down the wall for all flow rates used.

The procedure for a given experimental run was as follows. The tank was filled with uniformly salt-stratified fluid, and, when the fluid was at rest, the density profile was accurately measured by a traversing conductivity probe, which was calibrated at the top and bottom by samples measured in an Anton Paar densitometer. The inflow was then begun, with a constant flow rate for a given period of time that ranged between 45 s and 4 min, after which it was abruptly terminated by reinserting the removable barrier next to the gate. After sufficient time for the gravity waves and other motions in the tank to die away (typically 30 min), the density profile was again measured with the conductivity probe. This probe design has been used in many experiments at Aspendale (and elsewhere) for the past 25 years. The probe consists of a glass tube, which is lowered into the fluid at a constant rate. Fluid entering the tip of this glass tube is siphoned past two internal electrodes, where measured current records the conductivity. Up to four such profiles were taken before and after each run to ensure repeatability, and to confirm that the fluid was in fact stationary. Fourteen runs that met all these conditions were used for analysis. These had a variety of inflow rates, inflow densities and initial density gradients, and the details of these are given in table 1. The inflowing fluid was dyed with fluorescein, and illuminated in a thin central vertical section by a scanned beam from an Argon ion laser, which gave a clear picture of a two-dimensional cross-section of the motion. Each run (or most of it) was recorded on videotape for subsequent inspection and analysis. Representative

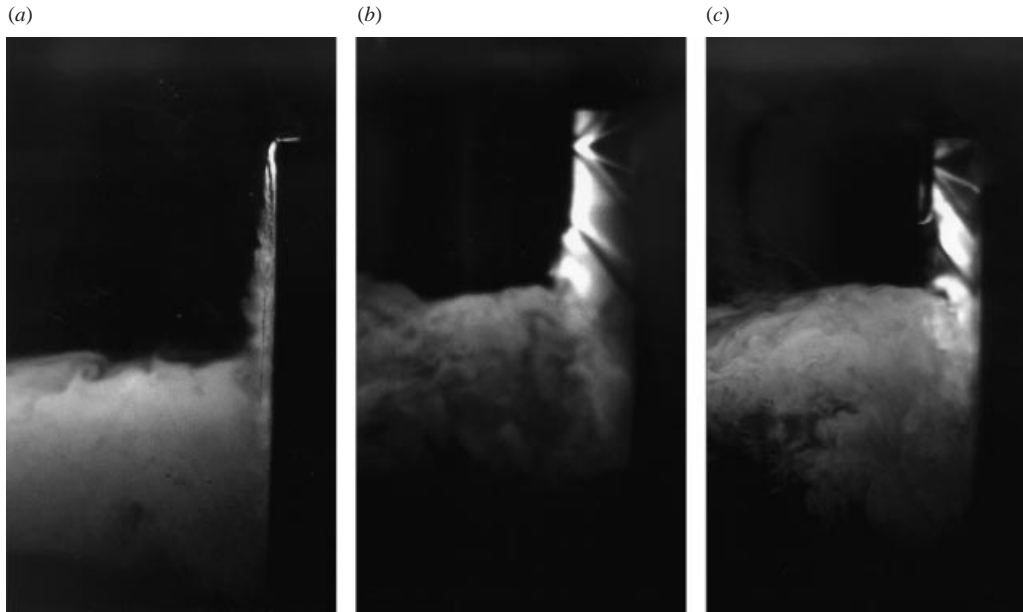


FIGURE 3. Photographs showing examples of three experiments, illuminated by a thin scanning laser beam, giving an instantaneous cross-section of the flow. The inflow is dyed with fluorescein and shows as light in colour. (a)  $B_0 = 0.0018$ ; (b)  $B_0 = 0.0423$ ; (c)  $B_0 = 0.0139$ . The vertical wall is on the right-hand side. A short vertical barrier 3 cm left of the wall (indicated in figure 2b) obscures the top of the plume in (b) and (c), and causes the variations in illumination in the plume.

photographs of the instantaneous flow for three different runs are shown in figure 3. The volume of the tank that lies behind the central barrier has the effect of increasing the effective length of the working region, as the initial and final profiles are the same as would be obtained if the working region were extended by a length appropriate to this volume. This permits a longer running time, minimizes the effect of start-up and shut-down, and permits the assumption that the conditions of the experiment are effectively constant throughout the run, although some allowance may be required for the small increase in overall depth.

The procedure of measuring the initial and final density profiles enables us to determine the amount of fluid that is deposited at each level of the tank, as described in Baines (1999, 2001). Figure 4 shows initial and final density profiles for a representative run. These profiles show how the level of each particular density value has moved vertically (generally upwards) as a result of the inflow and associated mixing.

### 3. Observations

The parameters that are fixed for each experimental run are: the volume flux  $Q_0$  of inflow per unit width of the tank, the density of the inflow  $\rho_i$ , the difference  $\Delta\rho_0$  in density between  $\rho_i$  and the ambient density  $\rho_0(0)$  at the level of the inflow, the ambient buoyancy frequency  $N$ , and the distance  $D$  below the level of the inflow at which the density of the inflow is equal to the ambient density (so that  $\rho_i = \rho_0(-D)$ ). To these we may add the kinematic molecular viscosity  $\nu$ , but our primary scaling is concerned with the previous parameters. The values of these parameters for the 14 runs are given in table 1. From these, we may define the dimensionless parameters  $B_0$ ,  $R_{p0}$  and  $Re$ , as defined by equations (1.1), (1.3) and (1.4).  $B_0 = 0$  for a homogeneous

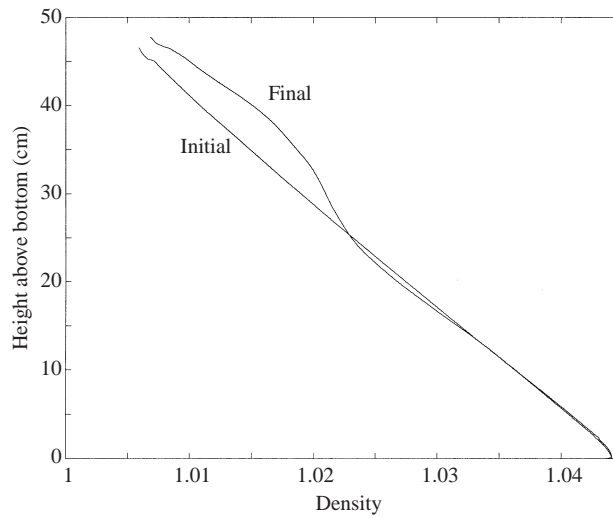


FIGURE 4. An example of initial and final environmental density profiles for a typical experiment ( $B_0 = 0.00925$ ). The difference between these profiles is used to infer the inflow and outflow caused by the plume.

environment, and its value increases with the stratification, although  $B_0 < 1$  for realistic flows. Note that the form of definition of  $B_0$  involving  $N$  enables it to have a local value using the local values of  $Q(z)$  and  $g'(z)$ , so that

$$B(z) = Q(z)N^3/g'(z)^2. \quad (3.1)$$

At the start of the inflow, the descending motion (visualized by fluorescein) has the form of a descending two-dimensional starting-plume structure (Tsang 1970; Turner 1973, p. 194), showing a rapidly descending initial downflow region, with a return-flow region outside it. After a few seconds, this head of the starting plume reaches its maximum extent, and subsequently the flow attains an approximately steady state, with turbulent fluctuations, that persists for the duration of the run (see figure 3). The downflow adjacent to the wall is initially laminar but quickly becomes turbulent, as seen in figure 3. In all observed runs, the width of this region increases very slightly with downward distance, and for practical purposes is approximately constant above the level  $z_1$ . This flow is steady in the mean, in that it is not disturbed by large meanders or eddies, except near the bottom where the downward motion ceases; here, there are fluctuations in the mean position of the maximum extent of this downflow. Mixing occurs in vigorous eddies owing to shear at the boundary of the downflow. Further away from the wall, there is upward motion in the lower regions, and this fluid rises toward a range of equilibrium levels indicated by the region of the dyed layer in the tank. The mean width  $\bar{d}$  of the region of the downflow adjacent to the wall is an observable parameter in the experiments. Its measurement is somewhat subjective, and has been based on visual observations of the width of the dyed layer, which is largely identified (approximately) with the region of mean downward motion. Some allowance for error must therefore be made of the order of  $\pm 10\%$ , but the repeatability of measurements indicates that the real error is less than this. Repeated observations and measurements give consistent results, and consequently we have confidence that this parameter and its value are meaningful. These enable



the definition of the pseudo-Richardson number

$$R_p = g' \bar{d}^3 / Q^2, \quad (3.2)$$

which is a function of  $z$ , with the starting value  $R_{p0}$ , equation (1.3), where  $Q$ ,  $\bar{d}$  and  $g'$  take their initial values. Values of  $\bar{d}$  and  $R_{p0}$  are also given in table 1. Observations of  $R_p$  taken above the level of  $z_1$  show that it decreases monotonically to small values as  $z$  decreases from 0 toward  $z_1$ , owing to increasing  $Q$  and decreasing  $g'$ . This behaviour contrasts with that of buoyant jets in homogeneous environments, in which  $R_p$  increases monotonically as the flow evolves into a plume (Kotsovinos & List 1977).

Observations and simple dynamical considerations show that the downflowing fluid adjacent to the vertical wall passes through a number of recognizable stages along its path. Initially, it has the character of an inertial jet, governed by the initial mass and momentum flux. As the buoyancy force takes effect, however, it quickly evolves toward the character of a turbulent plume, governed by the mass flux and buoyancy, where the initial conditions of the inflow have progressively less importance. In these experiments, the distance  $(Q_0^2/g_0')^{1/3}$  is of order 1 cm, so that this change occurs within a distance of several cm. Further down, as the ambient density progressively increases, the buoyancy force progressively decreases, and the plume tends to revert to the dynamical status of a jet in a neutral environment. The accumulated momentum in this downflow carries it on further, into the region where the buoyancy forces are upward instead of downward, and progressively causes the flow to decelerate to zero velocity. In this bottom region, the slowly moving fluid is deflected away from the wall, rises in a broad stream and spreads out over a range of heights between two levels denoted  $z_1$  (upper) and  $z_2$  (lower). These various different flow regimes are depicted in figure 1. The phenomena of 'overshoot' and 'springback' at the bottom of the flow are well-known properties of plumes in stratified environments, having been described by Morton *et al.* (1956) for axisymmetric plumes, and by Bloomfield & Kerr (1998) for fountains.

It is well known that mean velocity and density profiles in two-dimensional jets and plumes are approximately Gaussian, and in homogeneous environments each expands at a constant rate with downstream distance (Kotsovinos & List 1977; Chen & Rodi 1980; List 1982*b*), with spreading angles of  $5^\circ$ – $6^\circ$  based on velocity. This is consistent with dynamical similarity and an expansion in the scales of motion with downstream distance. Turbulent entrainment produces an inflow into the jet or plume, with increases its transport. The increase in width of the corresponding flows in stratified environments is comparable, but of generally smaller magnitude, as described above.

The analysis procedure used here is described in Baines (1999, 2001) and consists of taking the initial and final density profiles and differencing them to obtain the effective deposition of the inflowing fluid and its effect of the environment. The change in vertical elevation of each density surface, as a result of the inflow, gives a continuous representation of the flux of fluid that has penetrated to below that surface. Scaling this flux with  $Q_0$  gives the function  $\tilde{Q}(\rho)$ , and an example is shown in figure 5(*a*). From  $\tilde{Q}(\rho)$  we may calculate the net downward flow at a fixed height  $z$  from

$$Q(z) = Q_0 \int_{\rho_i(z)}^{\rho_f(z)} \tilde{Q}(\rho) d\rho / (\rho_f(z) - \rho_i(z)), \quad (3.3)$$

$$\approx \frac{1}{2} Q_0 (\tilde{Q}(\rho_i(z)) + \tilde{Q}(\rho_f(z))), \quad (3.4)$$

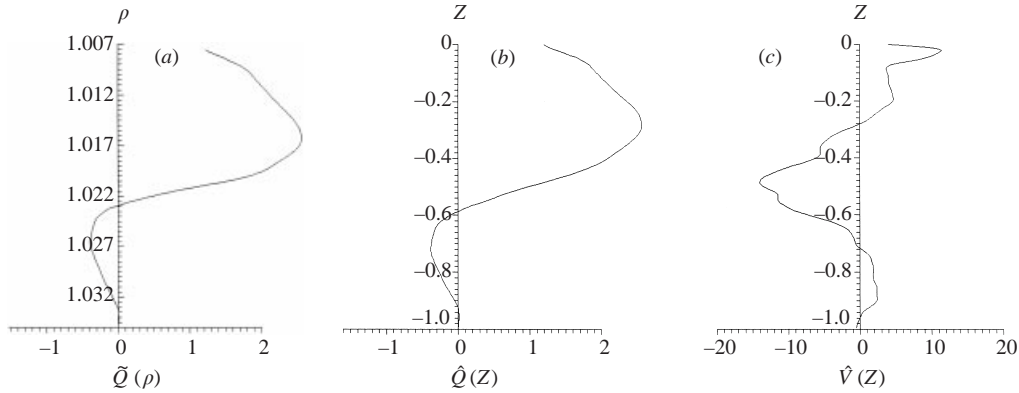


FIGURE 5. Representative examples of the functions  $\tilde{Q}(\rho)$ ,  $\hat{Q}(Z)$  and  $\hat{V}(Z)$ , for the run with  $B_0 = 0.00925$ . The first ( $\tilde{Q}(\rho)$ ) shows the downslope volume flux as a function of density, averaged over the whole downflow, and  $\hat{Q}(Z)$  and  $\hat{V}(Z)$  show the corresponding mean downslope volume flux in the current and outflow velocity, respectively, as functions of scaled depth  $Z = z/D$ . Positive values of  $\hat{V}(Z)$  denote flow toward the plume.

where  $\rho_i(z)$  and  $\rho_f(z)$  denote the initial and final density values at height  $z$ . Expressing this in terms of  $Z = z/D$ , we have

$$\hat{Q}(Z) = Q(z)/Q_0, \quad Z = z/D. \quad (3.5)$$

$\hat{Q}(Z)$  is therefore an appropriately stretched version of  $\tilde{Q}(\rho)$ . The mean outflow velocity  $v(z)$  from the downflow is then given by

$$v(z) = -\frac{dQ(z)}{dz}, \quad (3.6)$$

and in dimensionless form by

$$\hat{V}(Z) = v(z)D/Q_0 = -\frac{d\hat{Q}(Z)}{dZ}. \quad (3.7)$$

Examples of  $\hat{Q}(Z)$  and  $\hat{V}(Z)$  are shown in figures 5(b) and 5(c). Most results hereinafter are described in terms of the dimensionless coordinate  $Z$ , or its distance equivalent,  $S = -Z$ .

The information contained in  $\hat{Q}(Z)$  and  $\hat{V}(Z)$  describes the sum total of all mixing events inside and outside the plume, at each density level. In particular, it captures the sum of the effects of the downflowing plume, and its rising extension further away from the wall. Figure 6 shows representative  $\hat{Q}$  curves for a range of values of  $B_0$ . These show that in most experiments the net downward transport increases to an initial maximum, then decreases to zero and becomes negative (upward net flux), before decreasing to zero beyond depths to which the downflow has not penetrated. More revealing, perhaps, are the  $\hat{V}$  curves, which are reproduced individually for each run in figure 7. These show the two separate regions of net inflow into the downflow, separated by a central region of strong outflow. From these curves we may identify three significant heights for each, denoted  $Z_1$ ,  $Z_2$  and  $Z_3$ , as follows.  $Z_1$  denotes the uppermost or first level (below the origin) where  $\hat{V}(Z) = 0$ ; this coincides with the maximum in  $\hat{Q}$ .  $Z_2$  denotes the lower or second level where  $\hat{V}(Z) = 0$ , and  $Z_3$  marks the maximum penetration depth, as identified by the  $\hat{Q}$  and  $\hat{V}$  curves. Hence, the upper region of inflow lies above  $Z_1$ , the region of outflow lies between  $Z_2$  and  $Z_1$ ,

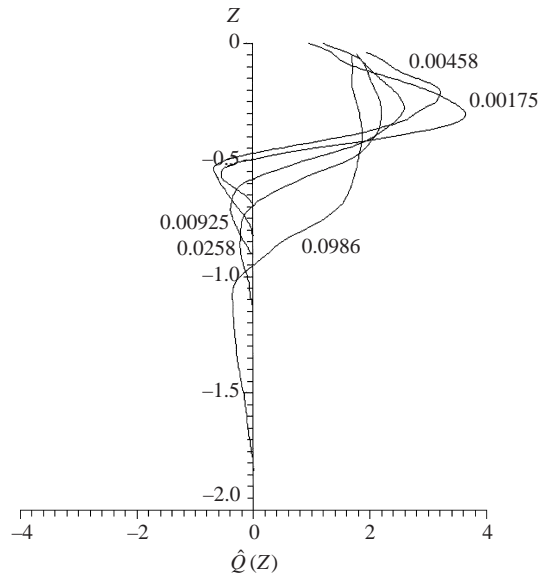


FIGURE 6. The downward volume flux in the plume  $\hat{Q}(Z)$  as a function of depth  $Z$  for a number of representative runs. Numbers attached to curves denote values of  $B_0$ .

and the lower region of inflow lies between  $Z_3$  and  $Z_2$ . The observed variations of these quantities with  $B_0$  are shown in figure 8(a). We note that  $Z_1$  is approximately uniform with increasing  $B_0$  (albeit with a slight decrease), but that  $Z_2$  and  $Z_3$  show a significant decrease (increase in magnitude) or descent, to below the initial level of  $Z = -1.0$ . The levels  $Z_1$  and  $Z_2$  correspond with the upper and lower boundaries of the dyed layer in the tank, as observed at the end of the run, and thereby mark the region of the net outflow. The fact that some values of  $Z_2$  are below the level of the inflow density (for  $M_0 \sim 0.1$ ) is a measure of the degree of entrainment into the plume in the overshoot region below this level. The values of  $\hat{Q}$  at  $Z = Z_1$  and  $Z_2$  are shown in figure 8(b), and these denote the maximum and minimum observed values of  $\hat{Q}$ . The maximum shows a generally decreasing trend with increasing  $B_0$ , which implies reduced entrainment into the downflow in the region above  $Z_1$ .  $\hat{Q}(Z_2)$ , on the other hand, has an approximately constant value of about  $-0.4$ . This represents the magnitude of the flux of the fluid that is entrained into the plume in the overshoot region, and carried up into the outflow region above  $Z_2$ ; this is uniform with  $B_0$  and about 40% of the magnitude of the initial inflow.

The  $\hat{V}$  curves show some interesting detailed structure. At small  $B_0$  (e.g. 0.00175) the upper inflow region shows two maxima in the inflow velocity, with the lower being the larger in amplitude and net inflow transport. As  $B_0$  increases, both peaks and the net entrainment decrease in amplitude, but the lower peak decreases more rapidly so that for values of  $B_0$  near 0.01, the upper peak is dominant. For larger  $B_0$  values, the two peaks are barely distinguishable, and there is effectively a single central peak. For the outflow region between  $Z_2$  and  $Z_1$ , for small  $B_0$  there is initially a large central peak, which decreases as  $B_0$  increases. A small upper second peak then appears, and persists for larger  $B_0$ . A third subsidiary peak in outflow begins to appear below the main one at  $B_0 = 0.00925$ , and then generally becomes progressively more important as  $B_0$  increases further. Possible reasons for these variations in the outflow are discussed in succeeding sections. Below  $Z_2$ , there is the inflow region

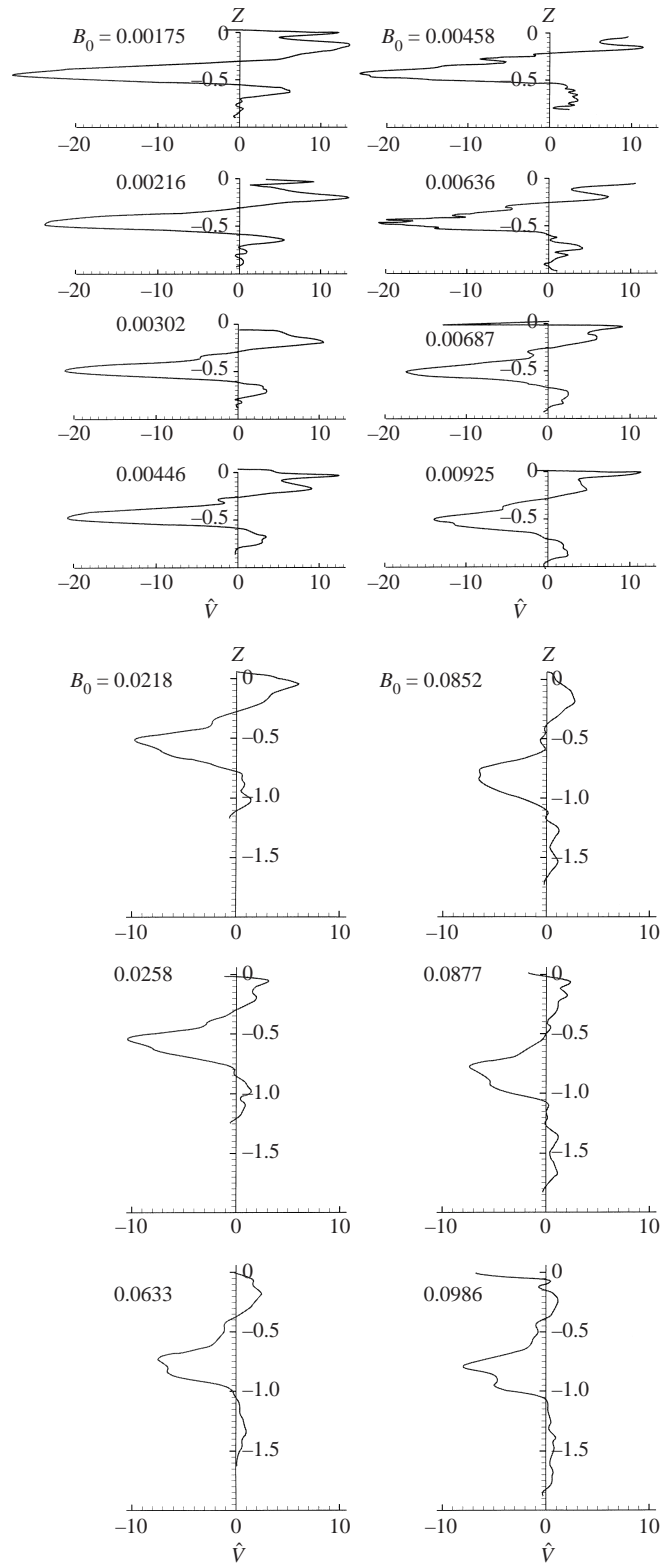


FIGURE 7. For caption see facing page.

associated with entrainment in the overshoot. For small  $B_0$ , this has a clear single peak, which decreases and broadens (vertically) as  $B_0$  increases, although the net entrainment remains approximately constant as noted above.

Finally, as noted above, the mean thickness of the downflowing stream is observed to increase very slowly with downslope distance, for each experiment. This is partly because the lower part of the plume (below  $z_1$ ) is obscured by the dyed fluid of the outflow resulting from springback. In any case, the value of  $\bar{d}$  observed immediately above  $z_1$  may be regarded as an observed mean value for the plume (in this region at least), and as shown in figure 9, has a dependence on  $B_0$  that can be reasonably well fitted with the power law relationship

$$\frac{\bar{d}}{D} = 0.62B_0^{0.48}. \quad (3.8)$$

The exponent here is very close to 0.5, and  $\bar{d}/D \sim B_0^{0.5}$  implies that

$$\bar{d} \sim (Q_0/N)^{1/2}. \quad (3.9)$$

This suggests that  $\bar{d}$  is affected by the external stratification. This may be so in these experiments, but the result may also be coincidental;  $N$  here only varies by a factor of two, and (3.9) cannot apply in the limit as  $N$  becomes small.

#### 4. Comparison with predictions from conventional plume models

Bulk models of plumes, both plane and axisymmetric, in homogeneous environments have consisted of equations for the fluxes of mass  $Q$ , of momentum  $M$  and of buoyancy  $F$ , integrated across the plume. From these, we may define the mean velocity  $U$  and the mean plume width  $\bar{d}$  by

$$Q = U\bar{d}, \quad M = U^2\bar{d}. \quad (4.1)$$

The buoyancy flux is then given by

$$F = QG, \quad (4.2)$$

where  $G$  is the mean buoyancy of the plume, defined by  $G \equiv g' \equiv g\Delta\rho/\rho_0$ . The principal physical factors involved are the buoyancy force and turbulent entrainment of environmental fluid into the plume. This involves two coefficients ( $E$  and  $P_2$ ) that are assumed to be dependent on dimensionless numbers, and, for two-dimensional buoyant jets, the controlling equations take the form (e.g. List 1982*b*)

$$\frac{dQ}{ds} = EU = EQ/\bar{d}, \quad (4.3)$$

$$\frac{dM}{ds} = \frac{d(Q^2/\bar{d})}{ds} = P_2G\bar{d} - C_D U^2 = P_2G\bar{d} - C_D Q^2/\bar{d}^2, \quad (4.4)$$

$$\frac{dF}{ds} = 0, \quad (4.5)$$

---

FIGURE 7. Profiles of the outflow function  $\hat{V}(Z)$ , obtained as the derivative of the curves in figure 6. The curves are characterized by their  $B_0$  values, given in the table. Negative values imply flow away from the wall.

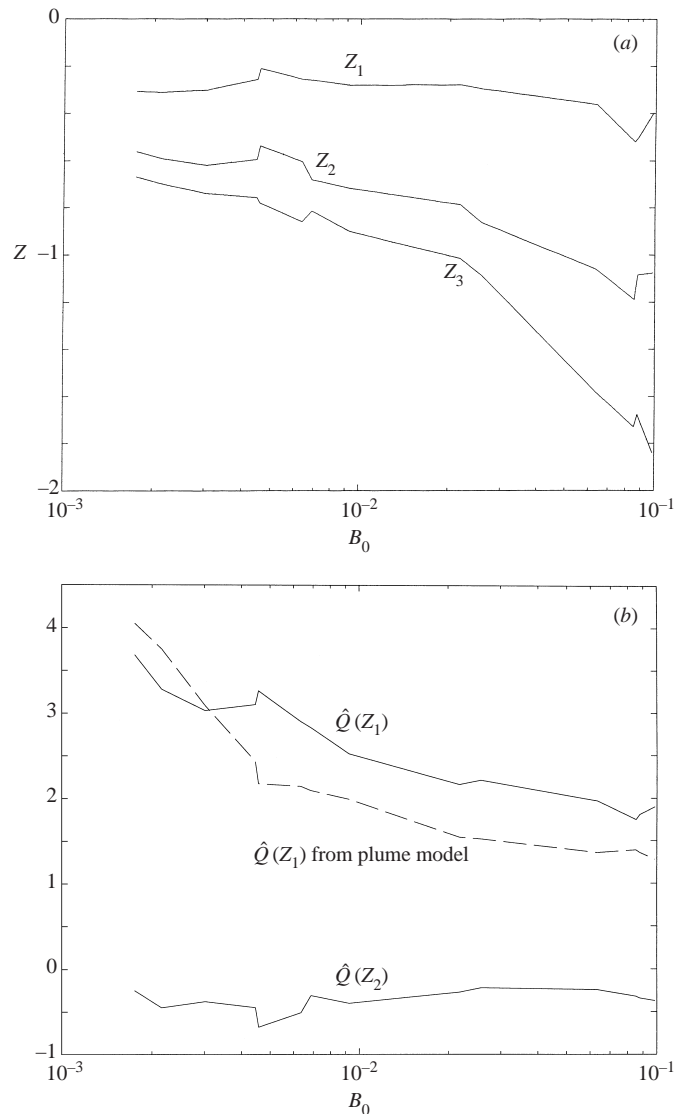


FIGURE 8. (a) The observed heights  $Z_1$ ,  $Z_2$  and  $Z_3$ , as functions of  $B_0$ , obtained from the curves of figure 7.  $Z_1$  and  $Z_2$  denote the upper and lower boundaries of the main outflow (where  $\hat{V}(Z) = 0$ ), and  $Z_3$  denotes the distance of maximum penetration, where again  $\hat{V}(Z) = 0$ . (b) Observed values of  $\hat{Q}(Z_1)$  and  $\hat{Q}(Z_2)$  as functions of  $B_0$ , giving a measure of the fluid entrained into the plume above  $Z_1$  and below  $Z_2$ . The dashed curve shows the value of  $\hat{Q}$  at the observed values  $Z_1$ , obtained from the model of § 4.

where  $s (= -z)$  is the coordinate in the direction of the initial motion,  $P_2$  is a constant shape factor, and  $E$  and  $P_2$  are functions of the local pseudo-Richardson number, as given by (3.2). The frictional drag of the vertical wall (where  $C_D$  is the drag coefficient) on the flow has been included here for completeness, but is generally small and is often neglected. These equations are based on a careful dimensional analysis of the various terms involved (List & Imberger 1973), and also assume that the mean transports within the plume are dominated by the mean motion rather than the turbulent fluxes.

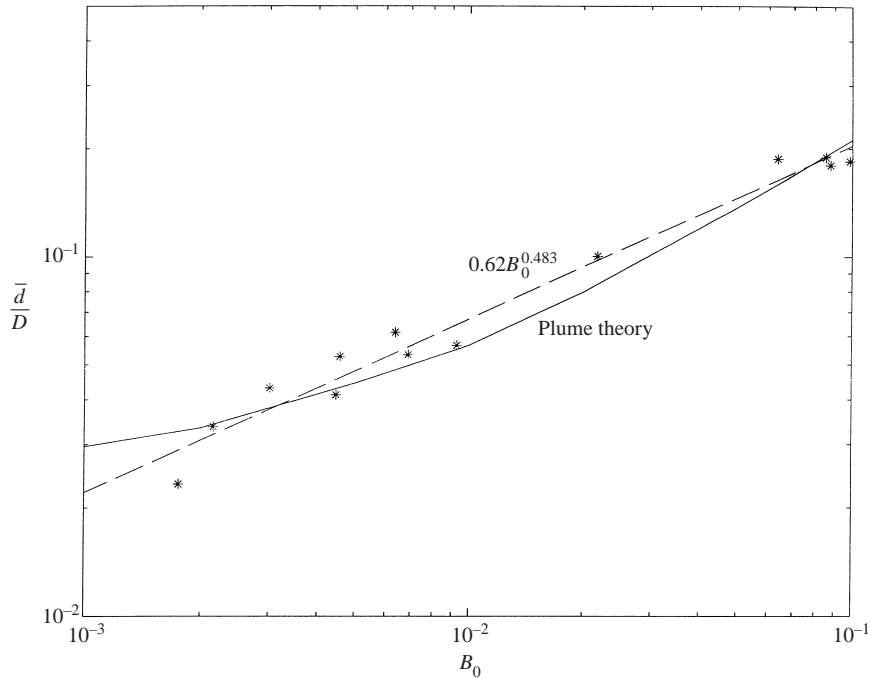


FIGURE 9. The observed mean thickness of the plume, measured shortly above the level  $Z = Z_1$ . These points have been fitted with the power law relationship  $\bar{d}/D = 0.62B_0^{0.483}$  (shown dashed). The solid curve denotes the value of  $\bar{d}/D$  at  $Z = -0.2$ , obtained from the model of §4 with  $\hat{d}(0) = 1$ .

Kotsovinos & List (1977) suggested that the latter may be significant, but this is now not generally accepted (Chen & Rodi 1980). These equations make no assumptions about the across-plume profiles of velocity and buoyancy, and are independent of them. The interpretations of  $U$  and  $\bar{d}$  in terms of real dimensions do depend on these profiles, but only by constant factors. The observed mean profiles in homogeneous environments are approximately Gaussian.

With a stratified environment, most authors have followed Morton *et al.* (1956), and used the same equations, with the last replaced by

$$\frac{dF}{ds} = -N^2Q, \quad (4.6)$$

which incorporates the effect of changing buoyancy due to the varying density of the background environment. Forms for  $P_2$  and  $E$  for two-dimensional isolated free buoyant jets in homogeneous environments were obtained by Kotsovinos & List (1977), and re-summarized by List (1982*b*). With the above definitions and for equations (4.4)–(4.6), these forms are

$$\begin{aligned} P_2 = 0.46, \quad E = 0.146(1 + R_p/R_{pp}) \quad (0 < R_p < R_{pp}) \\ = 0.292 \quad (R_p > R_{pp}), \end{aligned} \quad (4.7)$$

where the pseudo-Richardson number  $R_p = 0$  for a non-buoyant jet, and  $R_p$  approaches the constant value  $R_{pp} = 0.63$  as the flow approaches the state of a pure plume. For ‘wall jets’ such as those described here, where the flow is adjacent to a vertical barrier, the entrainment process is one-sided, so that the net entrainment is effectively halved. The mean profile of density in the wall jet is approximately a one-

sided half that of the symmetric free jet, so that for buoyant wall jets in homogeneous environments, for equations (4.4)–(4.6),  $P_2$  is unchanged, but  $E$  is half that above, and varies from 0.073 to 0.146. In the present experiments, the flow may begin as a jet, but then becomes a plume, and then a neutrally buoyant jet, and then a negatively buoyant plume, or fountain. Bloomfield & Kerr (1998) assumed that the entrainment coefficient  $E$  was constant in the fountain stage, and found that a value of 0.08 (i.e. 0.16 for two-sided entrainment) gave a reasonable fit to experiments with plane fountains. Accordingly, it is here assumed that  $E$  is constant in this region, taking the (similar) value 0.073—the same value as for plumes at zero values of  $R_p$ —so that  $E$  has the form

$$\begin{aligned} E &= 0.073 & (R_p < 0) \\ &= 0.073(1 + 1.59R_p) & (0 < R_p < 0.63) \\ &= 0.14 & (R_p > 0.63). \end{aligned} \quad (4.8)$$

$E$  has been evaluated experimentally from (4.3) for the range  $Z_1 < Z < 0$ , and although there is considerable scatter, the form of the mean of the observed values shows a monotonic increasing trend with  $R_p$  broadly consistent with (4.8), although the magnitudes are slightly larger. If we make the assumption that  $E$  is effectively constant, which is equivalent to the model of Morton *et al.* (1956), these equations may be solved by quadrature for given initial conditions, but this is not done here.

For present purposes it is convenient to take  $\bar{d}$ ,  $G$  and  $Q$  as the dependent variables, and to non-dimensionalize them in the form

$$S = \frac{s}{D} = -Z = -\frac{z}{D}, \quad \hat{d} = \frac{\bar{d}}{d_0}, \quad \hat{G} = \frac{G}{G_0}, \quad \hat{Q} = \frac{Q}{Q_0}, \quad (4.9)$$

where  $G_0 = G(0)$ ,  $Q_0 = Q(0)$ , are the initial values of  $G$  and  $Q$ , respectively, and  $d_0 = (Q_0^2/G_0)^{1/3}$ . The hypothesized equations for  $\hat{d}$ ,  $\hat{G}$  and  $\hat{Q}$  are then

$$\frac{d\hat{d}}{dS} = \frac{1}{B_0^{2/3}}(2E + C_D - P_2R_p), \quad (4.10)$$

$$\frac{d\hat{G}}{dS} = -\frac{N(S)^2}{N_0^2} - \frac{1}{B_0^{2/3}}E\frac{\hat{G}}{\hat{d}}, \quad (4.11)$$

$$\frac{d\hat{Q}}{dS} = \frac{1}{B_0^{2/3}}E\frac{\hat{Q}}{\hat{d}}, \quad (4.12)$$

where  $N_0^2 = G_0/D$ , and  $N(S)$  denotes variation in the buoyancy frequency with  $S$ . For the case of uniform  $N$ , as in these experiments,  $N(S) = N_0$ . The pseudo-Richardson number,

$$R_p = \frac{G\bar{d}^3}{Q^2} = \frac{\hat{G}\hat{d}^3}{\hat{Q}^2}, \quad (4.13)$$

with this scaling.

Apart from  $E$  and  $C_D$ , two dimensionless parameters are contained in this system, namely  $B_0$  and  $R_{p0}$ . The initial conditions for  $\hat{G}$  and  $\hat{Q}$  for these equations are then  $\hat{G}(0) = 1$ , and  $\hat{Q}(0) = 1$ , and the initial value of  $\hat{d}$ ,  $\hat{d}(0) = R_{p0}^{1/3}$ . It should be noted that  $\bar{d}$  may be scaled to include the factor  $B_0^{2/3}$ , but this is not preferred here because this scaling does not remove  $B_0$  from the equations. These equations have been solved



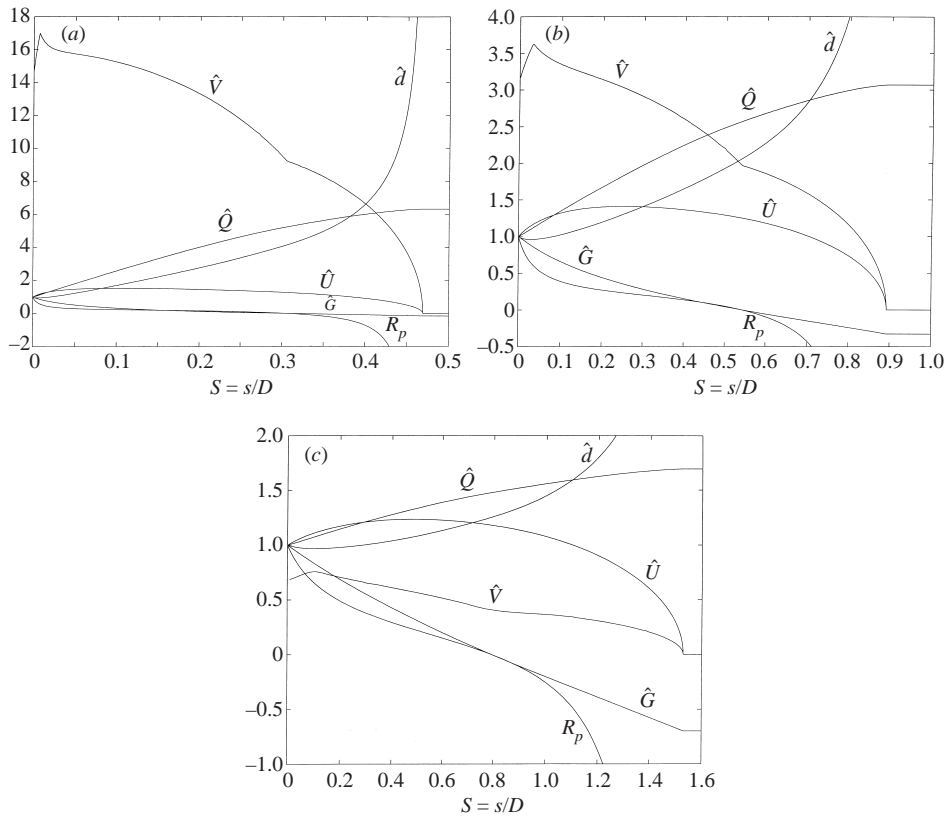


FIGURE 10. Examples of the solution  $(\hat{d}, \hat{G}, \hat{Q})$  of the model equations, (4.10)–(4.12), for the plume (a)  $B_0 = 0.001$ ; (b) 0.01, and (c) 0.1, with  $\hat{d}(0) = 1 = R_{p0}$ . Also shown are the pseudo-Richardson number  $R_p$ , the (scaled) mean downflow velocity  $\hat{U}$ , and entrained inflow velocity profile  $\hat{V}$ . The form of  $\hat{V}$  is similar to that of  $\hat{U}$  except near  $S = 0$ . Note that  $V = EU \ll U$ , but  $\hat{V} > \hat{U}$  because of scaling.

numerically using the routine ODE45 of MATLAB, for values of  $B_0$  ranging from 0.001 to 0.1, and  $R_{p0}$  ranging from  $10^{-3}$  to  $10^3$ . The solutions are generally insensitive to the value of  $R_{p0}$  unless  $R_{p0} < 0.1$ . In the experiments, the initial value of  $\hat{d}$  may be estimated from the values of  $R_{p0}$  given in table 1. These values are all of order unity or larger, and hence the solutions with  $R_{p0} = 1$  may be taken to be representative of the experiments. Three representative solutions for  $B_0 = 0.001, 0.01$  and 0.1 are shown in figure 10. These solutions provide profiles of  $\hat{d}, \hat{G}$  and  $\hat{Q}$  with height, the mean velocity  $\hat{U} = \hat{Q}/\hat{d}$ , the entrained inflow  $\hat{V} = d\hat{Q}/dS$ , and the pseudo-Richardson number,  $R_p$ . They also give the maximum penetration of the plume  $S_f$  (where  $\hat{U} = 0$ ) and the values of  $\hat{G}$  and  $\hat{Q}$  at this end point,  $\hat{G}_f$  and  $\hat{Q}_f$ , respectively. All of these values are representative of solutions with  $R_{p0} > 0.1$ , as is seen (for example) in figure 11, which shows a three-dimensional plot of  $\hat{Q}_f$  as a function of both  $B_0$  and  $R_{p0}$ . Clearly, the net entrainment over the distance of travel of the downflow increases substantially as  $B_0$  decreases. The same equations were also solved with the constant entrainment coefficient (as used by Morton *et al.* 1956; Bloomfield & Kerr 1998), with  $E = 0.073$ . The general pattern of the computed solutions is the same as those obtained using (4.8), because  $R_p$  decreases rapidly to small values when it is initially positive (see

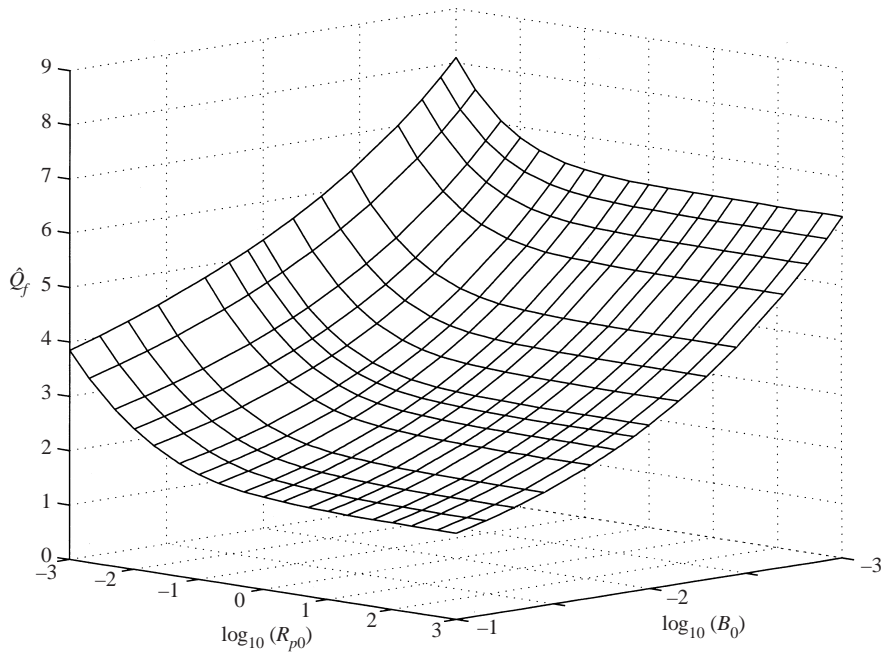


FIGURE 11. The total flux  $\hat{Q}_f$  at the endpoint  $Z_f$ , obtained from the plume model of §4. This represents the initial inflow (unity) plus all the fluid entrained into the plume along its length. Note that this is approximately independent of  $R_{p0}$  if  $R_{p0} > 0.1$ .

the curves for  $R_p$  in figure 10), but there are quantitative differences. The effects of changes to the drag coefficient are generally negligible provided that it is of the same order of magnitude as that assumed here (0.006).

Detailed comparisons between the profiles of entrainment and the observations are restricted to the following points by the presence of the springback of the fluid after leaving the plume. The theoretical entrainment decreases with increasing depth, which is consistent with the large observed inflows near the top of the plume, and the smaller inflows in the overshoot region at the bottom, as shown in figure 7. The turbulent plume described by the model can only be clearly seen in the experiments above the level  $Z_1$ , which from figure 8(a) has a mean position at approximately  $Z = -0.3$ . The value of  $\hat{Q}$  at the observed values of  $Z_1$  is shown in figure 8(b) for comparison with the observed values of  $\hat{Q}(Z_1)$ . In general, the trend of the two is consistent, but the model values are mostly smaller, indicating that the values of  $E$  used are smaller than those applicable to the experiment. Scaled with  $D$ , the observed plume thickness  $\bar{d}$  may be compared with the theoretical thickness calculated from the model (taking the value at  $Z = -0.2$ , which is above  $Z_1$  for all runs), and this is shown in figure 9. Again, the model gives a reasonably accurate description of  $\bar{d}$ , including its variation with  $B_0$ .

The level of maximum penetration of the plume  $Z_f = -S_f$ , may be compared with the observed value,  $Z_3$ ; this is done in figure 12, which shows consistent if not perfect agreement. For further comparison of these model results with the observations, some more assumptions are required. The model aims to describe a plume down to its level of maximum extent. Here, the buoyancy is now positive, and, after coming to rest, the fluid springs back to occupy and spread over a range of depths as described in the previous section. This springback process occurs away from the wall, and is

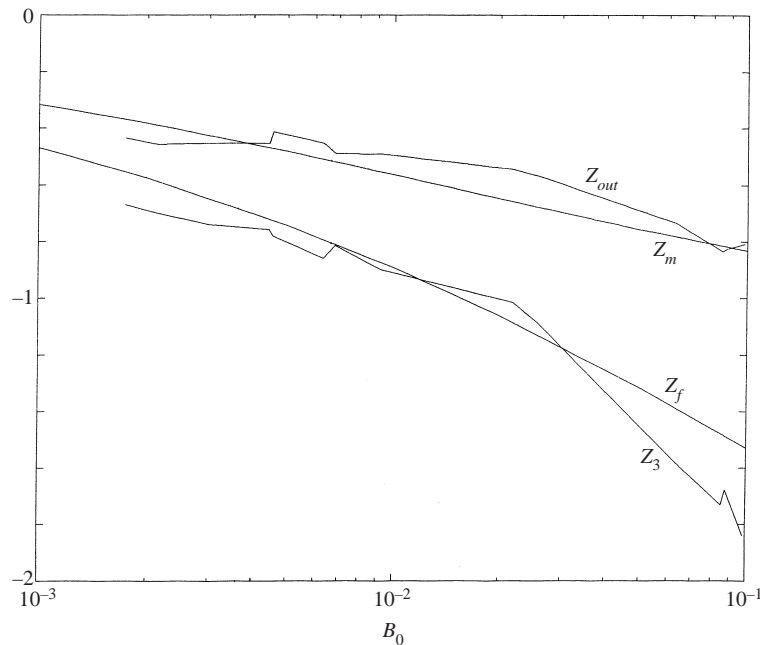


FIGURE 12. Comparison between observations and model predictions. The observed central level of the outflow ( $Z_{out}$ ) is compared with the prediction from the model of the level ( $Z_m$ ) of mean density of this outflow, identified with the density at the bottom of the plume, and assuming no mixing in the springback. Also, the observed maximum extent of plume fluid  $Z_3$  is compared with the theoretical prediction  $Z_f$ .

very different from the downflow in the plume. The latter has vigorous eddies and turbulence on the scale of  $\bar{d}$  and smaller, which cause the mixing and entrainment parameterized in the model. The springback process, on the other hand, is observed to have large length scales, and of itself, does not appear to generate many small scale eddies and, hence, little turbulent mixing. In other words, the continuous adjustment of a broad current of fluid moving up to its range of equilibrium levels under buoyancy does not promote the generation of the vigorous small-scale eddies required for mixing. One may therefore make the approximation that mixing associated with springback is negligible, and that the latter merely distributes the mixed fluid in the plume amongst the levels of its neutral density. Accordingly, the central level of the main outflow,  $Z_m$ , may be equated with the ambient level of the fluid at the bottom of the downflow, so that

$$Z_m = -S_f - \hat{G}_f, \quad (4.14)$$

and this may be compared with the observed central level of outflow,  $Z_{out}$ , where  $Z_2 < Z_{out} < Z_1$ .  $Z_{out}$  is approximately given by the peak of the outflow for negative  $\hat{V}$  in figure 7, but a more robust estimate is obtained by taking the median value (since the peak may be significantly off centre) over the range where  $\hat{V} < 0$ .  $Z_m$  and  $Z_{out}$  are compared in figure 12, and show good qualitative agreement, with very weak dependence on  $B_0$ .

With this conceptual picture of the overall dynamics, we may now make some inferences and speculations about the causes of the observed variations in the outflow (negative  $\hat{V}$ ) described in §3 and shown in figure 7. Here, a single maximum for  $B_0$  near 0.001 becomes three maxima when  $B_0$  approaches 0.1. There are two possible

reasons, or mechanisms, for these peaks. The first concerns the varying depth of the overshoot with  $B_0$ , and the second, variations in entrainment into the plume and the potential for the recycling of fluid after springback. For the first mechanism, for small  $B_0$ , the overshoot is quite small (distance  $\sim 0.1D$ ), and the outflow has a single peak. Here, the thickness of this outflow is a reflection of the variation in density of the fluid in the plume (because little mixing is expected from the springback process), which is expected to have an approximately Gaussian profile. However, as  $B_0$  increases, the maximum depth  $Z_3$  of the overshoot becomes larger, extending below  $-2$  as  $B_0$  approaches 0.1. This implies that the fluid entrained into the plume below  $Z_2$  comes from deeper in the environmental fluid, and hence becomes progressively more dense with increasing  $B_0$ . Also, below  $Z_2$ , observations of the flow show that not all the fluid in the plume reaches level  $Z_3$ , as some buoyant fluid tends to leave the outer parts of the descending plume in the range  $Z_3 < Z < Z_2$ . Together these processes must tend to produce non-Gaussian features in the variation of density of the total fluid entering the environment, and I suspect that they contribute to the lowest of the peaks observed in the outflow when  $B_0 > 0.05$ . The second likely mechanism concerns the variation in the entrainment with  $B_0$  and depth. Over the range of depths between  $Z_1$  and  $Z_2$ , the model implies that this entrainment is a maximum near  $Z_1$ , decreasing downwards. Fluid rising through springback to these levels may be re-entrained into the plume, carried downward by it, and then returned by springback and recycled, possibly many times. The net effect of this recycling would be to remove fluid systematically from the re-entrained levels near  $Z_1$ , and to redistribute it to other (lower) levels in the range  $(Z_2, Z_1)$  where entrainment is weaker. In other words, fluid near  $Z_1$  is removed from the environment and redistributed by the plume through springback to other preferred regions between  $Z_1$  and  $Z_2$ . This process is clearly capable of causing secondary peaks in the net outflow. It may well explain the minimum between the first and second peaks in  $\hat{V}$  that appears for  $B_0 > 0.003$ , which broadens into the reduced outflow in the upper part of the range  $(Z_2, Z_1)$  at large  $B_0$ .

## 5. Conclusions and discussion

I have described a set of laboratory experiments on two-dimensional vertical wall plumes into a stratified environment. The principal observational findings are as follows.

(i) When compared with flow types (jets, plumes) in a homogeneous environment, these plumes pass through a number of different dynamical stages or local flow types, as indicated in figure 1. First, the flow has the form of an inertial jet, which evolves into a buoyant plume, and then into a non-buoyant jet as the relative buoyancy decreases to zero. As the fluid descends beyond its (mean) equilibrium level, it then becomes a negatively buoyant plume, or 'fountain'. Throughout this path, environmental fluid is entrained into the 'plume', helping to maintain its mean position next to the vertical wall, until the buoyancy reversal causes the downward velocity to decrease to zero. The presence of the wall prevents large-scale meanders that are found in isolated plane buoyant jets (Kotsovinos 1977).

(ii) The mean width  $\bar{d}$  of the main initial downflow increased slowly with depth, in common with the more familiar behaviour of jets and plumes in homogeneous environments. Concomitant with this, the downflow is observed to entrain fluid from the environment as is customary for jets and plumes.

(iii) The fluid in the plume appears to descend to near the termination point  $Z_3$

(though not all of it reaches  $Z_3$ ), and then ‘springs back’ to finally occupy and outflow in a range of heights between  $Z_1$  and  $Z_2$ , which depend on the mixing of the initial plume fluid. This ‘springback’ process is an important part of the overall flow, and has a major impact on the final disposition of the inflowing fluid. The flow has the appearance of a heavily damped oscillator, with no further vertical fluctuations being visible after the initial ‘springback’.

(iv) The flows can be characterized by the initial value of the buoyancy number,  $B_0 = Q_0 N^3 / g_0^2$ . In terms of the vertical scale  $D$ , all depths  $Z_1$ ,  $Z_2$  and  $Z_3$  increase with  $B_0$ . The mean observed width  $\bar{d}$  is approximately given by equation (3.8),  $\bar{d}/D = 0.62 B_0^{1/2}$ , which implies  $\bar{d} \sim (Q_0/N)^{1/2}$ .

(v) The observations show interesting double-peaked structure in the entrained inflow to the plume in the upper part of the flow. There is also a double-peaked structure in the outflow when  $B_0 > 0.01$ , which becomes more prominent as  $B_0$  increases further. These features are not contained in the model, and some possible causes are described in §4.

(vi) Observations of  $\dot{Q}$  at  $Z_1$  and  $Z_2$  show that the entrained fluid above  $Z_1$  decreases with  $B_0$ , but below  $Z_2$ , the total rate of entrainment of environmental fluid into the plume, carried upward by springback, is roughly constant with  $B_0$ , and is equal to 40% of the initial inflow,  $Q_0$ .

The overall properties have been compared with the predictions of the ‘standard model’, based on bulk equations for mass, momentum and buoyancy flux for the downflow. This is essentially the same model as that used by Morton *et al.* (1956) and Bloomfield & Kerr (1998), with the exceptions that the model includes a drag coefficient for the sidewall, and the entrainment coefficient  $E$  contains a dependence on pseudo-Richardson number (following List & Imberger 1973) with a slightly different numerical value. The effect of the drag coefficient term is small, but the variation of  $E$  introduces quantitative differences. No parameter values (such as the entrainment coefficient) were adjusted to optimize agreement with observations. In addition to the usual plume model assumptions, the assumption was made that nearly all mixing was associated with the vigorous eddies caused by shear at the boundary of the downflow, and that negligible mixing occurred in the large-scale springback. Qualitative agreement was found between this model and the main observables, indicating that the physics of the flow were correctly represented. The plume width, the level of the main outflow and the depth of maximum penetration are all reasonably well described by the model, including the variation of these quantities with  $B_0$ . However, the observed entrainment is larger than that assumed here in the model, and there are notable differences in detail, such as double peaks in the main outflow for values of  $B_0$  greater than 0.01, and other differences seen in figure 12. These indicate that the model has its limitations and should be used with care. The assumption of negligible mixing during springback is reasonable, but has yet to be tested. It is possible that  $E$  and  $P_2$  contain some dependence on  $B$ , but this has not been examined here.

The reason why plumes entrain at all is reasonably clear. A one-sided plume may be compared with two fluid streams of unequal velocity that are initially separated by a splitter plate. If this plate disappears at some point so that the two streams make contact and start to mix, a spreading mixing layer forms between them. If coordinates are taken with one of the streams at rest, the mixing layer has the effect of entraining this stationary fluid into the moving stream, in the manner observed and modelled in jets and plumes. The properties of these flows may be contrasted with

those observed down gentle slopes ( $\leq 12^\circ$ ) into stratified environments, described by Baines (2001). In the latter, a two-way exchange between the fluid in the downflow and the environment occurs, in which some fluid is detrained from the current and other fluid is entrained into it. The detrainment is generally larger than the entrainment. The difference between these two flow types may be traced to the form of growing disturbance arising from shear flow instability, and consequent turbulent eddy production. In the vertical plume case, the profiles of density and velocity approximately coincide, resulting in a form of Kelvin–Helmholtz instability, primarily due to the shear between the environment and the downflow. This produces eddies on a range of length scales that are in locations that can mix the fluid effectively, and this mixing region broadens with distance downward. The kinematics of flows with a mixing region that broadens with downflow distance then dictates that environmental fluid is effectively entrained into the downflow. For the downslope flows on gentle slopes, however, the process is more akin to Holmboe instability, where the strongest vorticity gradient (of negative sign) is situated above the region of strongest density gradient (Baines 2001). Instability results from the interaction of waves on this vorticity gradient with waves on the density interface (see for example Baines (1995, §4.8)). The resulting eddies are strongest in the upper region, above the density interface, and their displacement from the region of large density variations reduces their mixing potential. Hence, in the plume case the eddies mix strongly, and the plume is turbulent and diffusive, resulting in net entrainment, whereas on gentle slopes the upper boundary of the downslope current maintains its identity and sharp interface, with reduced entrainment and net fluid loss to the environment.

The author is most grateful to David Murray for his customary careful assistance with all aspects of the experiments. The paper has also benefited from some insightful comments by three referees. The change in nomenclature from the parameter  $M$  to the buoyancy number  $B$  was made after discussions with the referees and editor. This choice was adopted in the interests of improving terminology in the subject and maintaining consistency in notation. The term ‘pseudo-Richardson number,  $R_p$ ’ was introduced for the same reasons.

#### REFERENCES

- BAINES, P. G. 1995 *Topographic Effects in Stratified Flows*. Cambridge University Press, 482pp.
- BAINES, P. G. 1999 Downslope flows into stratified environments—structure and detrainment. In *Mixing and Dispersion in Stably Stratified Flows*. Proc. 5th IMA Conf. on Stratified Flows (ed. P. Davies), pp. 1–21. Clarendon Press, Oxford.
- BAINES, P. G. 2001 Mixing in flows down gentle slopes into stratified environments. *J. Fluid Mech.* **443**, 237–270.
- BLOOMFIELD, L. J. & KERR, R. C. 1998 Turbulent fountains in a stratified fluid. *J. Fluid Mech.* **358**, 335–356.
- CHEN, C. J. & RODI, W. 1980 *Vertical Turbulent Buoyant Jets—a Review of Experimental Data*. Pergamon, 79pp.
- ELLISON, T. H. & TURNER, J. S. 1959 Turbulent entrainment in stratified flows. *J. Fluid Mech.* **6**, 423–448.
- KILLWORTH, P. D. 1979 On ‘chimney’ formations in the ocean. *J. Phys. Oceanogr.* **9**, 531–554.
- KOTSOVINOS, N. E. 1977 Plane turbulent buoyant jets. Part 2. Turbulence structure. *J. Fluid Mech.* **81**, 45–62.
- KOTSOVINOS, N. E. & LIST, E. J. 1977 Plane turbulent buoyant jets. Part 1. Integral properties. *J. Fluid Mech.* **81**, 25–44.
- LIST, E. J. 1982a Turbulent jets and plumes. *Annu. Rev. Fluid Mech.* **14**, 189–212.

- LIST, E. J. 1982*b* Mechanics of turbulent buoyant jets and plumes. In *Turbulent Buoyant Jets and Plumes*, W. Rodi (ed.). Pergamon.
- LIST, E. J. & IMBERGER, J. 1973 Turbulent entrainment in buoyant jets and plumes. *J. Hydraul. Div. ASCE* **99**, 1461–1474.
- MORTON, B. R., TAYLOR, G. I. & TURNER, J. S. 1956 Turbulent gravitational convection from maintained and instantaneous sources. *Proc. R. Soc. Lond. A* **234**, 1–23.
- PALMER, M. R. & ERNST, G. G. J. 1998 Generation of hydrothermal megaplumes by cooling of pillow basalts at mid-ocean ridges. *Nature* **393**, 643–647.
- PRIESTLEY, C. H. B. & BALL, F. K. 1955 Continuous convection from an isolated source of heat. *Q. J. R. Met. Soc.* **81**, 144–157.
- ROUSE, H., YIH, C.-S. & HUMPHREYS, H. W. 1952 Gravitational convection from a boundary source. *Tellus* **4**, 201–210.
- TSANG, G. 1970 Laboratory study of two-dimensional starting plumes. *Atmos. Environ.* **4**, 519–544.
- TURNER, J. S. 1973 *Buoyancy Effects in Fluids*. Cambridge University Press, 367 pp.
- TURNER, J. S. 1986 Turbulent entrainment: the development of the entrainment assumption, and its application to geophysical flows. *J. Fluid Mech.* **173**, 431–471.